CORE
Metadata, citation and similar papers at core.ac.uk
Provided by Online Research Database In Technology

Technical University of Denmark

Efficiency enhancement of InGaN amber MQWs using nanopillar structures

Ou, Yiyu; Iida, Daisuke; Liu, Jin; Wu, Kaiyu; Ohkawa, Kazuhiro; Boisen, Anja; Petersen, Paul Michael; Ou, Haiyan

Published in:
Nanophotonics

Link to article, DOI:
10.1515/nanoph-2017-0057

Publication date:
2018

Document Version
Publisher's PDF, also known as Version of record

Link back to DTU Orbit

Citation (APA):
Ou, Y., Iida, D., Liu, J., Wu, K., Ohkawa, K., Boisen, A., ... Ou, H. (2018). Efficiency enhancement of InGaN amber MQWs using nanopillar structures. Nanophotonics, 7(1), 317-322. DOI: 10.1515/nanoph-2017-0057

DTU Library
Technical Information Center of Denmark

General rights
Copyright and moral rights for the publications made accessible in the public portal are retained by the authors and/or other copyright owners and it is a condition of accessing publications that users recognise and abide by the legal requirements associated with these rights.

- Users may download and print one copy of any publication from the public portal for the purpose of private study or research.
- You may not further distribute the material or use it for any profit-making activity or commercial gain
- You may freely distribute the URL identifying the publication in the public portal

If you believe that this document breaches copyright please contact us providing details, and we will remove access to the work immediately and investigate your claim.

Research article

Yiyu Ou*, Daisuke Iida, Jin Liu, Kaiyu Wu, Kazuhiro Ohkawa, Anja Boisen, Paul Michael Petersen and Haiyan Ou

Efficiency enhancement of InGaN amber MQWs using nanopillar structures

https://doi.org/10.1515/nanoph-2017-0057
Received May 18, 2017; revised June 26, 2017; accepted July 1, 2017

Abstract: We have investigated the use of nanopillar structures on high indium content InGaN amber multiple quantum well (MQW) samples to enhance the emission efficiency. A significant emission enhancement was observed which can be attributed to the enhancement of internal quantum efficiency and light extraction efficiency. The size-dependent strain relaxation effect was characterized by photoluminescence, Raman spectroscopy and time-resolved photoluminescence measurements. In addition, the light extraction efficiency of different MQW samples was studied by finite-different time-domain simulations. Compared to the as-grown sample, the nanopillar amber MQW sample with a diameter of 300 nm has demonstrated an emission enhancement by a factor of 23.8.

Keywords: InGaN MQWs; nanopillar; QCSE; strain relaxation; light extraction.

1 Introduction

In the past few decades, research in III-nitride compound semiconductors has achieved outstanding breakthroughs, leading to the commercialization of InGaN multiple quantum well (MQW)-based blue light-emitting diodes (LEDs) [1–4]. InGaN MQW-based LEDs are capable of emitting in the full visible spectral range by adjusting the indium content. Extremely high external quantum efficiency (EQE) larger than 80% has already been achieved on blue LEDs [5]. Meanwhile, the EQE of longer-wavelength LEDs (green, yellow, red) is still relatively lower than for blue devices. For longer-wavelength LEDs with high indium content, the internal quantum efficiency (IQE) is mainly limited by the large spontaneous polarization and piezoelectric polarization induced by the large compressive strain in MQWs, leading to the spatial separation of electrons and holes, known as the quantum confined Stark effect (QCSE) [6–10]. Thus, increasing the indium incorporation into InGaN growth will increase the internal strain, which results in a lower IQE and more severe QCSE. It is also known that high-crystal-quality InGaN with large indium content is difficult to grow, owing to the large lattice mismatch and low-temperature growth of MQWs (below 700°C) [11].

Recently, research in applying different strain compensation techniques in the growth processes has been investigated in order to suppress internal strain in InGaN MQWs [12, 13]. As a post-growth method, the fabrication of nanostructures on LEDs is acknowledged as an effective way to relieve internal stain in MQWs thanks to their small hetero-interfacial areas. It could also enhance the light extraction efficiency (LEE) due to increased surface scattering and diffraction from the nanostructures [14–16]. In the present work, we use nanopillar structures on InGaN amber MQWs with an emission peak at 637 nm to enhance the emission efficiency. Nanopillars of various sizes were fabricated on amber MQW samples via e-beam lithography and a top-down dry etching method. The size-dependent internal strain relaxation and emission intensity of nanopillar MQWs have been studied.

2 Sample preparation

InGaN amber MQW samples were grown via metal-organic vapor phase epitaxy (MOVPE) in a single-wafer horizontal

***Corresponding author: Yiyu Ou,** DTU Fotonik, Technical University of Denmark, Ørsteds Plads 343, DK-2800, Lyngby, Denmark, e-mail: yiyo@fotonik.dtu.dk. http://orcid.org/0000-0002-2127-9827
Daisuke Iida and Kazuhiro Ohkawa: Electrical Engineering, King Abdullah University of Science and Technology, Thuwal 23955-6900, Kingdom of Saudi Arabia
Jin Liu: School of Physics, Sun-Yat sen University, Guangzhou 510275, China
Kaiyu Wu and Anja Boisen: DTU Nanotech, Technical University of Denmark, DK-2800, Lyngby, Denmark
Paul Michael Petersen and Haiyan Ou: DTU Fotonik, Technical University of Denmark, DK-2800, Lyngby, Denmark

Open Access. © 2017 Yiyu Ou et al., published by De Gruyter. BY-NC-ND This work is licensed under the Creative Commons Attribution-NonCommercial-NoDerivatives 4.0 License.
Brought to you by | DTU - Technical Information Center of Denmark (DTIC)
Authenticated
Download Date | 11/15/17 2:32 PM

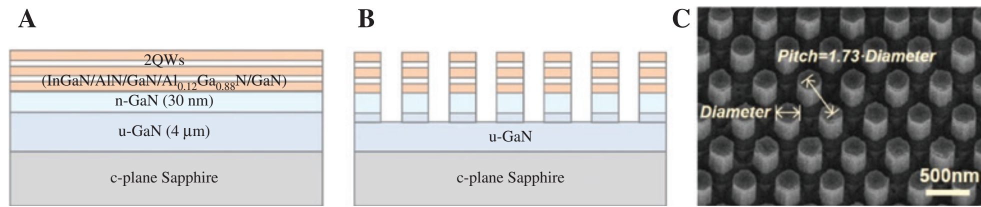

Figure 1: Schematic views of (A) the as-grown InGaN-based MQW structure and (B) the fabricated nanopillar structure, and (C) a bird-view SEM image of nanopillar MQWs (sample NP300 nm).

reactor system with a microflow channel at 100 kPa. Using this special microflow channel MOVPE [17], the growth temperature of InGaN MQWs can be raised to 740°C, which leads to an improved IQE performance. A tensile-strained AlN layer and AlGaN layers were introduced as barrier layers in the growth process in order to compensate for the compressive strain in the InGaN layer. The epitaxial structure consisted of a 4-μm-thick un-doped GaN layer grown on a (0001) c-plain sapphire substrate, a 30-nm-thick n-GaN layer, and a two-period 2.2-nm-thick $In_{0.33}Ga_{0.67}N$ MQW layer with the combination of 1.8-nm-thick AlN interlayers and 24-nm-thick (Al)GaN barrier layers, as illustrated in Figure 1A. MQW and AlN interlayers were grown at 740°C, and GaN and AlGaN barrier layers were grown at 850°C. The higher growth temperature for barrier layers can improve the crystalline quality of MQWs [18].

To fabricate the nanopillar structure, a 110 nm SiO_2 layer was first deposited as an interlayer on the amber MQW sample by plasma-enhanced chemical vapor deposition. Then a positive e-beam resist (PMMA) layer was spun on the SiO_2 surface. By using e-beam lithography with a subsequent development process, the designed pattern was transformed to the PMMA layer. A 30-nm-thick hard mask material (chromium) layer was then deposited on the PMMA layer by e-beam evaporation. Followed by a lift-off process in remover 1165 solution, patterned chromium was formed. A dry etching process was applied to transfer the pattern from chromium to SiO_2 by reactive-ion etching with a gas mixture of SF_6/O_2. The amber MQW sample was further etched down to the u-GaN layer by inductively coupled plasma (ICP) etching with a gas mixture of $Cl_2/Ar/BCl_3$. Finally, the residual SiO_2 was removed by buffer oxide etchant and the sample was treated in KOH solution to cure the ICP-induced etching damages on the structure sidewall. Nanopillar structures were obtained with the designed pattern as illustrated in Figure 1B.

A batch of six nanopillar arrays, samples NP70 nm, NP100 nm, NP300 nm, NP500 nm, NP700 nm and NP900 nm, were fabricated with a structure size (cross-sectional diameter of the nanopillar) of 70 nm, 100 nm, 300 nm, 500 nm, 700 nm and 900 nm, respectively. All the nanopillar structures were in hexagonal arrangement and the pitch/diameter ratio was fixed to 1.73. In addition, a structure height of 450 nm was achieved in the ICP etching process for all the samples. Figure 1C shows a bird-view scanning electron microscope (SEM) image of the sample NP300 nm as an example of fabricated nanopillar structures.

3 Experiments and results

Photoluminescence (PL) measurements were performed at room temperature to characterize the emission properties of different nanopillar samples and a plain as-grown sample as reference. A 405 nm laser was used as the optical excitation source and the signal was collected by an optical spectrometer (Instrument System CAS140, München, Germany), both of which were integrated to a microscope system. Both the excitation and collection were conducted from the top surface of the samples, and the excitation power density was 13.2 W/cm^2. The surface reflection of the excitation laser beam has been taken into account and the PL spectra are shown in Figure 2A. It is seen that the plain amber MQW sample has an emission peak at 637 nm and all the nanopillar samples demonstrate a significant emission enhancement. When the nanopillar size decreases from 900 nm to 70 nm, the emission intensity increases first and then decreases. The largest emission enhancement of 23.8 times is obtained on the sample NP300 nm. The observed emission enhancement can be attributed to two possible reasons: one is the enhanced IQE thanks to the strain relaxation in MQWs and alleviated QCSE, while the other is enhanced LEE because of the enhanced surface scattering and diffraction of the nanopillar structures.

Besides the emission enhancement, one can also see that all the nanopillar samples demonstrate a blue shift of the emission peak wavelength. The emission peak wavelength shifts toward shorter wavelength with decreased nanopillar size; meanwhile, the full width at half maximum (FWHM) of the emission peaks decreases, which is shown in Figure 2B. It is known that the large compressive strain in the MQW layer caused by the lattice

Brought to you by | DTU - Technical Information Center of Denmark (DTIC)
Authenticated
Download Date | 11/15/17 2:32 PM

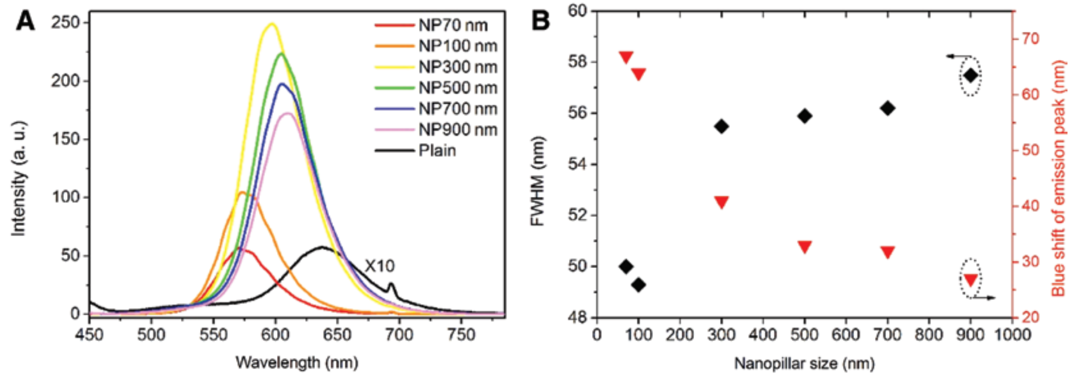

Figure 2: (A) PL spectra of different nanopillar samples and plain reference sample. The spectra are obtained under identical measurement conditions and the surface reflection of excitation laser beam has been taken into account. (B) Emission peak wavelength and FWHM of PL spectra as a function of the nanopillar size.

mismatch can be released by the fabrication of the nanopillar [14–16]; therefore, the strain-induced piezoelectric polarization could be reduced, which leads to an increased wavefunction overlap of electrons and holes. This results in an enhanced radiative recombination rate and IQE. The smaller nanopillar size corresponds to a larger blue shift of the emission peak which suggests a larger strain relaxation. In addition, the decrease of FWHM is attributed to the reduction of potential tilt in the MQWs thanks to the strain relaxation [19].

To further consolidate the strain relaxation effects, Raman scattering spectra of different samples were acquired at room temperature by using a DXRxi Raman imaging microscope system (Thermo Scientific, Waltham, MA, USA). The excitation source was a 633 nm laser beam focused to a spot size of 1.2 µm with 8 mW power. Raman spectra of the samples are shown in Figure 3, in which the E_2 (high) phonon mode is used to represent the in-plane stress in the MQW layer. One can observe that the E_2(H) phonon mode shifts toward lower wavenumbers when the nanopillar size decreases. The Raman shifts of the test samples can be given by $\omega_{E2(H)} = \omega_0 + C\sigma$, where ω_0 is the Raman shifts for stress-free GaN (568.0 cm^{-1}), C is the biaxial strain coefficient (–2.25 cm^{-1}/GPa for GaN), and σ is the in-plane compressive stress [20–22].

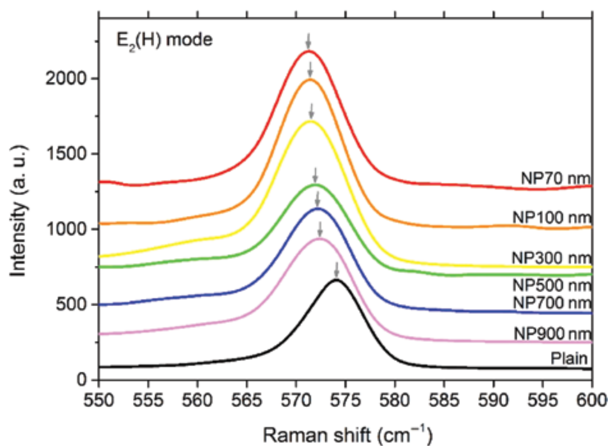

Figure 3: Raman spectra of the E_2(H) phonon mode of different nanopillar samples.

The E_2(H) phonon mode of different samples were identified from the Raman spectra and the corresponding in-plane compressive stresses σ were deduced and are listed in Table 1. It is shown that in-plane stress can be released in nanopillar samples compared to the plain sample, and a larger strain relaxation occurs in a smaller nanopillar sample. The largest strain relaxation of about 48.6% (from –2.76 GPa to –1.42 GPa) is obtained on the NP70 nm sample. This result affirms that strain relaxation has taken place in the nanopillar MQW samples and the smaller nanopillar structure leads to a larger strain relaxation which is in good agreement with the blue shift of the PL emission peak.

Time-resolved photoluminescence (TR-PL) measurements were performed using a time-correlated single photon counting system and a 375 nm pulsed laser with a pulse width of 44 ps as an excitation source (PicoQuant, Berlin, Germany). The excitation power density was 0.66 W/cm^2. The TR-PL decay curves were acquired at room temperature for all the samples, and the results are shown in Figure 4. A standard two-exponential-component model was used to study the decay dynamics, and the decay

Table 1: Raman shifts for the E_2(H) phonon mode and in-plane compressive stress σ of different nanopillar samples.

Nanopillar size (nm)	70	100	300	500	700	900	Plain
$\omega_{E2(H)}$ (cm^{-1})	571.2	571.4	571.5	571.9	572.1	572.3	574.2
σ (GPa)	−1.42	−1.51	−1.56	−1.73	−1.82	−1.91	−2.76

Brought to you by | DTU - Technical Information Center of Denmark (DTIC)
Authenticated
Download Date | 11/15/17 2:32 PM

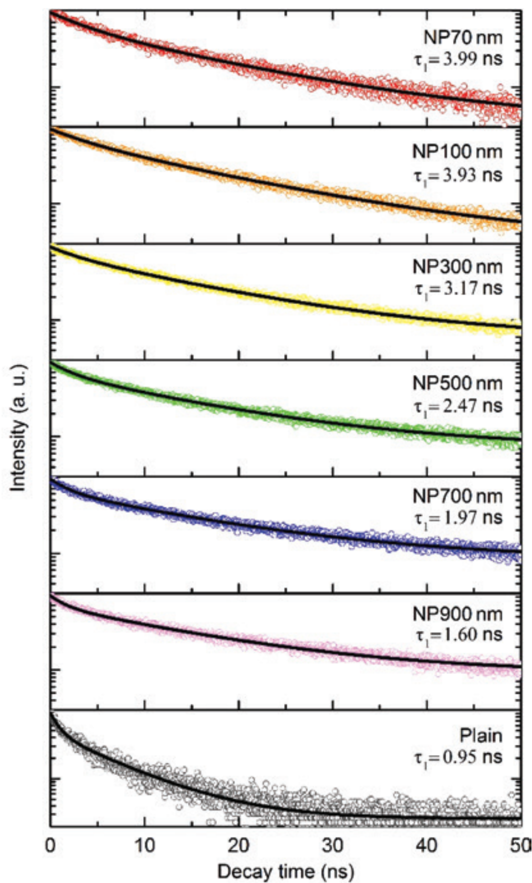

Figure 4: TR-PL decay curves for different samples acquired at room temperature.
The solid lines are the fitting results from the two-exponential-component model.

curves can be described by $I(t) = A_1\exp(-t/\tau_1) + A_2\exp(-t/\tau_2)$ [23], where $I(t)$ is the PL intensity as a function of time, A_1 and A_2 are constants, and τ_1 and τ_2 represent fast and slow decay lifetime, respectively. The fast decay lifetime corresponds to the rapid carrier recombination in MQWs, which is determined by both radiative and non-radiative recombination processes [24]. The fitted curves are also demonstrated in Figure 4, which shows that the fast decay lifetime τ_1 of all the nanopillar samples is longer than that of the plain sample. The much longer τ_1 indicates that the non-radiative recombination process has been suppressed significantly because of the large strain relaxation [25]. It is also seen that τ_1 becomes longer with decreased nanopillar size, which suggests an increased radiative recombination rate and thus a larger IQE enhancement for a smaller nanopillar structure.

From these results, one can see that the larger strain relaxation in MQWs does not necessarily lead to a larger emission enhancement. It is because the EQE enhancement of the MQW sample depends not only on its IQE enhancement but also on the LEE enhancement. To investigate the light transmission behavior through nanopillar structures of different sizes, a finite-different time-domain (FDTD, Lumerical Solutions, Vancouver, Canada) simulation was applied. A plane-wave excitation source from the substrate side was used and the size-dependent light propagation of nanopillar and plain samples were examined; the calculated transmittance spectra are shown in Figure 5. It is noted that the light transmittance is not equivalent to the total LEE of MQWs; however, the main LEE enhancement contribution of such a nanopillar MQW structure is achieved in the vertical direction [20]. Therefore, it is believed that the light transmittance behavior can give a good suggestion of the change of LEE. For the amber MQW samples, a high light transmittance is desired at its emission peak wavelength. The calculated transmittance of the samples at each corresponding emission wavelength is 0.833, 0.844, 0.993, 0.926, 0.918, 0.878 and 0.828 for the samples with increased nanopillar size (from NP70 nm to plain), respectively. In Figure 5, one can see that the local maximum of the light transmittance shifts toward shorter wavelength when the nanopillar size decreases. Sample

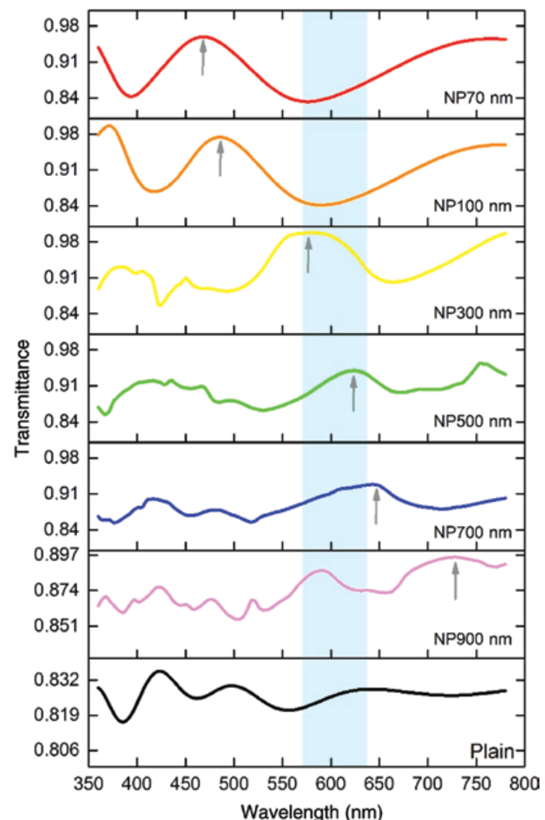

Figure 5: Calculated light transmittance spectra of different MQW samples; cyan region represents the range of emission wavelength (570–637 nm).

Brought to you by | DTU - Technical Information Center of Denmark (DTIC)
Authenticated
Download Date | 11/15/17 2:32 PM

Table 2: Nanopillar density and sidewall surface area of different MQW samples.

Nanopillar size (nm)	70	100	300	500	700	900	Plain
Nanopillar density (1/μm²)	78.5	38.5	4.3	1.5	0.8	0.5	0
Sidewall surface area (normalized to NP900 nm)	12.9	9	3	1.8	1.3	1	0

NP300 nm and NP500 nm have their local maximum of the light transmittance fallen in the emission wavelength range of the amber MQW samples (cyan area: 570–637 nm). These results are consilient with the PL results where the NP300 nm and NP500 nm samples show the first and second largest emission enhancement, respectively.

Besides the IQE and LEE, several other factors would also affect the emission intensity of the nanopillar samples. The nanopillar structures were fabricated by the top-down etching method which reduces the volume of the active region and then leads to a decreased emission intensity. For the fixed pitch/diameter ratio of 1.73 and the fixed structure height, the same filling factor (emission volume ratio of the nanopillar to plain sample) value of 0.302 is obtained for all the nanopillar samples, which suggests an about 70% decrease of the emission volume.

It is known that the surface damage as a non-radiative recombination channel was usually introduced during the dry etching process and the density of surface damage depends on the total surface area of the nanopillar sidewall [26]. The structure density of the nanopillar and the sidewall surface area (which is normalized to the one of the NP900 nm sample) have been calculated for all the samples and are listed in Table 2. It is noted that the nanopillar density increases when the nanopillar size decreases. Meanwhile, the total surface area of the nanopillar sidewall also increases. It increases dramatically when the nanopillar size is smaller than 300 nm, while the surface area of the NP70 nm sample is about 12 times larger than that of the NP900 nm sample. Such a large surface area for small nanopillar samples could lead to a more severe surface damage and limit the IQE enhancement. Therefore, it is worth mentioning that a surface passivation process, as we applied in this work, is essential to cure the surface damage and suppress the related non-radiative recombination process [19, 27, 28].

4 Conclusions

In summary, we have fabricated nanopillar structures for InGaN amber MQWs via e-beam lithography and the dry etching process. Nanopillar samples have different sizes (70–900 nm), and the size-dependent emission properties were studied. Compared to the as-grown sample, nanopillar samples demonstrate a significant emission enhancement which could be attributed to several reasons. One is the enhanced IQE owing to the strain relaxation of nanopillar structures. It is found that a larger strain relaxation occurs in a nanopillar sample with a smaller size, and this was confirmed by both blue shift of the PL emission peak and the downshift of the E_2(H) mode in the Raman spectra. TR-PL result indicates that a larger strain relaxation could lead to an increased radiative recombination rate. In addition, FDTD simulation has demonstrated that the light transmittance depends on the nanopillar size. A coincidence of the emission peak wavelength and local maximum of light transmittance (such as the NP300 nm and NP500 nm samples) could suggest a high LEE. Furthermore, the influence of the filling factor and surface damage of the nanopillar samples on the emission intensity has also been discussed. One can see that applying nanopillar structures is an effective approach to enhance the emission efficiency of a high indium content InGaN MQW sample. By carefully designing the nanopillar size, an emission enhancement of 23.8 times has been achieved on the amber MQW sample in this work.

Acknowledgments: This work was supported by the Innovation Fund Denmark (project no. 4106-00018B). KW and AB acknowledge support from the Danish National Research Foundation and Villum Foundation's Center for Intelligent Drug Delivery and Sensing Using Microcontainers and Nanomechanics (IDUN).

References

[1] Schubert EF, Kim JK. Solid-state light sources getting smart. Science 2005;308:1274–8.
[2] Pimputkar S, Speck JS, DenBaars SP, Nakamura S. Prospects for LED lighting. Nat Photon 2009;3:180–2.
[3] Amano H, Sawaki N, Akasaki I, Toyoda Y. Metalorganic vapor phase epitaxial growth of a high quality GaN film using an AlN buffer layer. Appl Phys Lett 1986;48:353–5.
[4] Nakamura S. GaN growth using GaN buffer layer. Jpn J Appl Phys 1991;30:L1705.
[5] Narukawa Y, Ichikawa M, Sanga D, Sano M, Mukai T. White light emitting diodes with super-high luminous efficacy. J Phys D Appl Phys 2010;43:354002.
[6] Miller DA, Chemla DS, Damen TC, et al. Band-edge electroabsorption in quantum well structures: the quantum-confined Stark effect. Phys Rev Lett 1984;53:2173.

Brought to you by | DTU - Technical Information Center of Denmark (DTIC)
Authenticated
Download Date | 11/15/17 2:32 PM

[7] Chichibu SF, Uedono A, Onuma T, et al. Origin of defect-insensitive emission probability in In-containing (Al, In, Ga) N alloy semiconductors. Nat Mater 2006;5:810–6.

[8] Wang T, Bai J, Sakai S, Ho JK. Investigation of the emission mechanism in InGaN-based light-emitting diodes. Appl Phys Lett 2001;78:2617–9.

[9] Kwon MK, Kim JY, Kim BH, et al. Surface-plasmon-enhanced light-emitting diodes. Adv Mater 2008;20:1253–7.

[10] Tsai YL, Lai KY, Lee MJ, et al. Photon management of GaN-based optoelectronic devices via nanoscaled phenomena. Prog Quant Electron 2016;49:1–25.

[11] Bai J, Wang Q, Wang T. Characterization of InGaN-based nanorod light emitting diodes with different indium compositions. J Appl Phys 2012;111:113103.

[12] Saito S, Hashimoto R, Hwang J, Nunoue S. InGaN light-emitting diodes on c-face sapphire substrates in green gap spectral range. Appl Phys Exp 2013;6:111004.

[13] Hwang JI, Hashimoto R, Saito S, Nunoue S. Development of InGaN-based red LED grown on (0001) polar surface. Appl Phys Exp 2014;7:071003.

[14] Geng C, Wei T, Wang X, Shen D, Hao Z, Yan Q. Enhancement of light output power from LEDs based on monolayer colloidal crystal. Small 2014;10:1668–86.

[15] Li S, Waag A. GaN based nanorods for solid state lighting. J Appl Phys 2012;111:5.

[16] Li KH, Zang KY, Chua SJ, Choi HW. Embedding nano-pillar arrays into InGaN light-emitting diodes. Physica Status Solidi C 2014;11:742–5.

[17] Ohkawa K, Watanabe T, Sakamoto M, Hirako A, Deura M. 740-nm Emission from InGaN-based LEDs on c-plane sapphire substrates by MOVPE. J Cryst Growth 2012;343:13–6.

[18] Iida D, Lu S, Hirahara S, Niwa K, Kamiyama S, Ohkawa K. Enhanced light output power of InGaN-based amber LEDs by strain-compensating AlN/AlGaN barriers. J Cryst Growth 2016;448:105–8.

[19] Zhu J, Wang L, Zhang S, et al. The fabrication of GaN-based nanopillar light-emitting diodes. J Appl Phys 2010;108:074302.

[20] Dong P, Yan J, Zhang Y, et al. Optical properties of nanopillar AlGaN/GaN MQWs for ultraviolet light-emitting diodes. Opt Exp 2014;22:A320–7.

[21] Puech P, Demangeot F, Frandon J, et al. GaN nanoindentation: a micro-Raman spectroscopy study of local strain fields. J Appl Phys 2004;96:2853–6.

[22] Perlin P, Jauberthie-Carillon C, Itie JP, San Miguel A, Grzegory I, Polian A. Raman scattering and x-ray-absorption spectroscopy in gallium nitride under high pressure. Phys Rev B 1992;45:83.

[23] Liu B, Smith R, Athanasiou M, Yu X, Bai J, Wang T. Temporally and spatially resolved photoluminescence investigation of $(11\bar{2}2)$ semi-polar InGaN/GaN multiple quantum wells grown on nanorod templates. Appl Phys Lett 2014;105:261103.

[24] Zhang G, Guo X, Ren FF, et al. High-brightness polarized green InGaN light-emitting diode structure with Al-coated p-GaN grating. ACS Photon 2016;3:1912–8.

[25] Liu B, Smith R, Bai J, Gong Y, Wang T. Great emission enhancement and excitonic recombination dynamics of InGaN nanorod structures. Appl Phys Lett 2013;103:101108.

[26] Li Q, Westlake KR, Crawford MH, et al. Optical performance of top-down fabricated InGaN/GaN nanorod light emitting diode arrays. Opt Exp 2011;19:25528–34.

[27] Zhao C, Ng TK, Prabaswara A, et al. An enhanced surface passivation effect in InGaN/GaN disk-in-nanowire light emitting diodes for mitigating Shockley-Read-Hall recombination. Nanoscale 2015;7:16658–65.

[28] Choi WH, You G, Abraham M, et al. Sidewall passivation for InGaN/GaN nanopillar light emitting diodes. J Appl Phys 2014;116:013103.

Brought to you by | DTU - Technical Information Center of Denmark (DTIC)
Authenticated
Download Date | 11/15/17 2:32 PM